A New 6D Chaotic Generator: Computer Modelling and Circuit Design

Michael Kopp[1,*], Andrii Kopp[2]

[1]Institute for Single Crystals, The National Academy of Sciences of Ukraine, Kharkiv, Ukraine

[2]National Technical University "Kharkiv Polytechnic Institute", Kharkiv, Ukraine

Received 01 June 2022; received in revised form 16 April 2022; accepted 17 April 2022

DOI: https://doi.org/10.46604/ijeti.2022.9601

Abstract

The objective of this study aims at using the Matlab-Simulink environment and the LabVIEW software environment to build computer models of a six-dimensional (6D) chaotic dynamic system. For the fixed system's parameters, the spectrum of Lyapunov exponents and the Kaplan-York dimension are calculated. The presence of two positive Lyapunov exponents demonstrates the hyperchaotic behavior of the system. The fractional Kaplan-York dimension indicates the fractal structure of strange attractors. An active control method is extended to achieve global chaotic synchronization of two identical novel 6D chaotic systems with unknown system parameters. Based on the results obtained in Matlab-Simulink and LabVIEW models, a chaotic signal generator for the 6D chaotic system is implemented in the MultiSim environment. The experimental results show that the chaotic behavior simulation in the MultiSim environment is similar to those in the Matlab-Simulink and LabVIEW models. The simulation results demonstrate that the Pecora-Carroll method is a simple way of chaotic masking and signal decoding.

Keywords: chaotic behavior, chaos generator, computer simulation, circuit simulation

1. Introduction

It is well known that dynamic chaos electronic generators are widely used in telecommunication systems [1-2], noise location systems [3], cryptography [4], neural network systems [5], and other applications. Recently, the design of new dynamic chaos electronic generators has been rapidly developing. Many circuit solutions are known for the classical equations of dynamic chaos [6-7].

Two major approaches can be designated for constructing electronic circuits of chaotic oscillators. One is the implementation of chaotic dynamics at a qualitative level, without requiring an exact formal correspondence to the equations. Here, simple radio engineering elements are usually used, containing transistors, diodes, etc. The other is the circuitry reproduction of the nonlinear dynamics equations. Here, it uses elements for analog modeling (integrators, multipliers, adders, etc.).

The development of new electronic dynamic chaos generators has been accelerating recently. Electronic chaos generators are based on Rössler equations [8], Rikitake equations [9], modified Lorentz equations [10-13], and Rucklidge equations [14]. Recently, new systems with hyperchaotic oscillations have been developed, such as Liu systems [15-16], Chen systems [17], and new modifications of the Lorentz equations [18-19] and Rikitake equations [20-22]. The book of Tlelo-Cuautle et al. [23] is devoted to an overview of chaos generators based on circuit simulation using the MultiSim package. Such systems are characterized by broadband, orthogonality, and complexity of the chaotic signal structure, as well as strong sensitivity to initial conditions. These properties determine perspectives for their use for the secure transmission of information.

* Corresponding author. E-mail address: michaelkopp0165@gmail.com

In this work, the reproduction approach is applied to the equations of six-dimensional (6D) chaotic dynamics. These equations were obtained in a study of convection in a nonuniformly rotating electrically conductive fluid in a constant vertical magnetic field [24]. The derivation of these equations is similar to the Lorentz equations [6], where the representation of physical fields was used as the expansion of the minimum order Fourier series. However, in contrast to the Lorentz equations (three-dimensional (3D)), a nonlinear dynamic system of equations that describes the higher phase space dimension (6D) is obtained [24].

Chaotic systems with an attractor of dimensions above 3D have a much wider practical application. It is preferred to use chaotic systems of a higher dimension for secure communication. The presence of more than one Lyapunov exponent leads to more complex chaotic system dynamics, which increases the security of information transmission. In addition, broadband, orthogonality, and complexity of the chaotic signal structure, as well as strong sensitivity to initial conditions, are the characteristics of such systems. These features define the opportunities for the application of such systems in secure information transfer. Therefore, computer simulation of chaotic signals is an important problem, and so does the search for a circuit implementation of chaotic oscillation generators.

The purpose of this study is to construct computer models of a 6D chaotic dynamic system using the Matlab-Simulink environment and the LabVIEW software environment. For the circuit implementation of the new chaos generator, the NI MultiSim package is used, where the chaotic dynamics is illustrated by signal oscillograms and phase portraits of attractors. This work suggests a scheme for chaotic modulation secure communication based on chaotic synchronization of a new 6D chaotic system. The proposed chaotic masking and signal decoding scheme is implemented through the analog electronic circuit, which is characterized by its high accuracy and good robustness.

2. Simulation of Chaotic Dynamics Equations in Matlab-Simulink and LabVIEW

2.1. Basic equations

The following shows the dynamic system of equations describing weakly non-linear convection in a nonuniformly rotating electrically conductive fluid in a constant magnetic field [24]:

$$\begin{cases} \dot{X} = -X + RY - TV - HU \\ \dot{V} = -V + HW + \sqrt{Ta}\,(1+Ro)X \\ \dot{U} = -Pm^{-1}U + Pr^{-1}X \\ \dot{W} = -Pm^{-1}W - Pr^{-1}V + Ro\sqrt{Ta}U \\ \dot{Y} = Pr^{-1}(-Y + X - XZ) \\ \dot{Z} = Pr^{-1}(-bZ + XY) \end{cases} \tag{1}$$

where the dot above the symbol indicates the differentiation with respect to time $\tilde{t}$. X and V are amplitudes of velocity field disturbances. U and W are amplitudes of magnetic field disturbances. Y and Z are amplitudes of temperature field disturbances. H, Ta, T, Pm, Pr, Ro, and b are real constants, and R (the Rayleigh number) is a bifurcation parameter. The nonlinear system of Eq. (1) has the dimension of a 6D phase space. Eq. (1) has a huge variety of multiple behavior modes. More likely, it can realize all possible transitions to chaos depending on the area of various dimensionless parameter changes. In the work of Kopp et al. [24], a dynamic analysis of the system in Eq. (1) was performed, and the existence of periodic, quasi-periodic, and chaotic regimes was proved depending on the values of the Rayleigh number.

Using the values of the parameters $Ta = 1080$, $T = 0.1$, $Pm = 1$, $Pr = 10$, $b = 8 / 3$, $Ro = -3 / 4$, and $H = 2$, the system in Eq. (1) can be written in a more convenient form for modeling:

$$\begin{cases} \dot{x}_1 = -x_1 + Rx_2 - 2x_4 - 0.1x_5 \\ \dot{x}_2 = \frac{1}{10}\left(-x_2 + x_1 - x_1x_3\right) \\ \dot{x}_3 = \frac{1}{10}\left(-\frac{8}{3}x_3 + x_1x_2\right) \\ \dot{x}_4 = -x_4 + \frac{1}{10}x_1 \\ \dot{x}_5 = -x_5 + 8.21x_1 + 2x_6 \\ \dot{x}_6 = -x_6 - 24.65x_4 - \frac{1}{10}x_5 \end{cases} \quad (2)$$

Here, new variables are introduced: $x_1 = X$, $x_2 = Y$, $x_3 = Z$, $x_4 = U$, $x_5 = V$, and $x_6 = W$. Eq. (2) is supplemented with initial conditions [24]: $x_1(0) = x_2(0) = x_3(0) = x_4(0) = x_5(0) = x_6(0) = 1$. Eq. (2) contains one parameter R, which allows considering a one-parameter set of solutions. The Rayleigh number R depends on the temperature difference at the boundaries of the electrically conductive fluid layer. By changing the heating conditions at the boundaries of the fluid layer (the Rayleigh number), it is possible to study various modes of convective instability.

2.2. Lyapunov exponents and Kaplan-Yorke dimension

One of the important criteria characterizing the chaotic behavior of a nonlinear dynamical system is the spectrum of Lyapunov exponents. With the help of the Lyapunov exponents, the rate of trajectory convergence or divergence in the phase space is determined. The presence of at least one positive value in the spectrum of Lyapunov exponents indicates the presence of chaotic oscillations in the system. The number of Lyapunov exponents corresponds to the dimension of the nonlinear dynamical system's phase space. For the system in Eq. (2), the number of such indicators is six.

The method of calculating Lyapunov exponents based on the Benetinn algorithm is used [25-26]. Following the works of Sandri [27] and Binous et al. [28], the maximum Lyapunov exponent for the system in Eq. (2) is calculated at $R = 58$: $L_{max} = 0.101898$. Then, using the Gram-Schmidt orthogonalization, all the Lyapunov exponents are precisely determined as follows: $L_1 = 0.0988591$, $L_2 = 0.0109865$, $L_3 = –0.544226$, $L_4 = –1.00557$, $L_5 = –1.15581$, and $L_6 = –1.77091$.

It can be seen that the spectrum of Lyapunov exponents has two positive terms (L_1 and L_2), so the system in Eq. (2) shows hyperchaotic behavior. The maximum Lyapunov exponent of the new hyperchaotic system (Eq. (2)) corresponds to the value $L_{1max} = 0.0988591$. The sum of the Lyapunov exponents in Eq. (2) is negative, which shows that the hyperchaotic system (Eq. (3)) is dissipative.

$$L_1 + L_2 + L_3 + L_4 + L_5 + L_6 = -4.36667 < 0 \quad (3)$$

The Kaplan-York dimension (KYD) of the new hyperchaotic system (Eq. (2)) is calculated as:

$$D_{KY} = 2 + \frac{L_1 + L_2}{|L_3|} \approx 2.20184 \quad (4)$$

This shows the high complexity of the system in Eq. (2). Fig. 1 depicts the dynamics of the Lyapunov exponents of the hyperchaotic system (Eq. (2)).

A comparison of various chaotic systems with the new chaotic system (Eq. (1) or (2)) is given in Table 1. Table 1 outlines existing systems, i.e. Lorenz [7] (and the modified [10, 18]), Rossler [8], Rikitake [9] (and the modified [21]), Rucklidge [14], and Lu [15] compared to a new chaotic system (Eq. (1)).

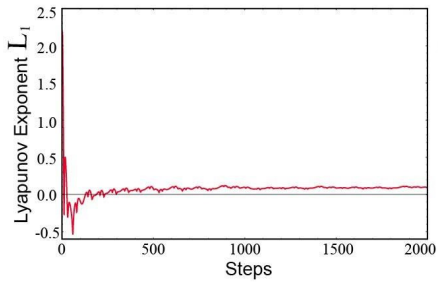

(a) Plot of the Lyapunov exponent L_1

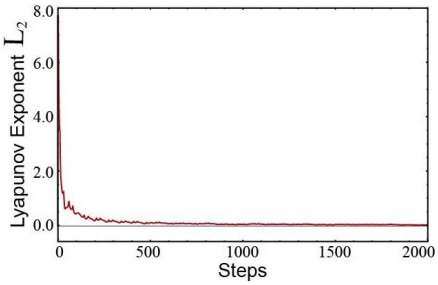

(b) Plot of the Lyapunov exponent L_2

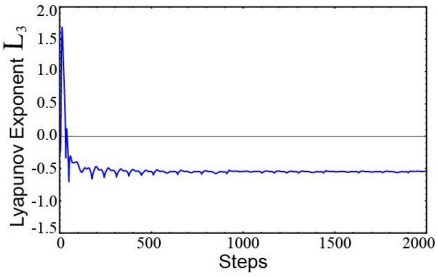

(c) Plot of the Lyapunov exponent L_3

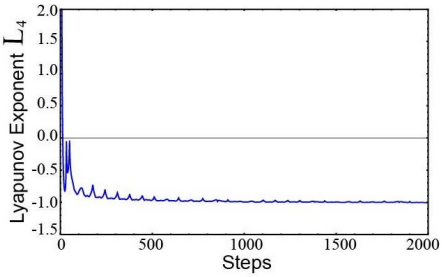

(d) Plot of the Lyapunov exponent L_4

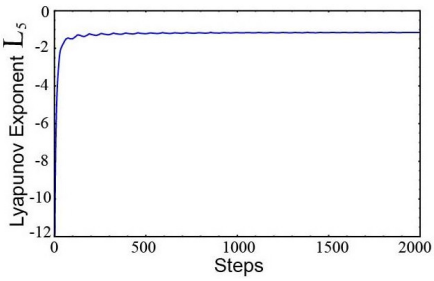

(e) Plot of the Lyapunov exponent L_5

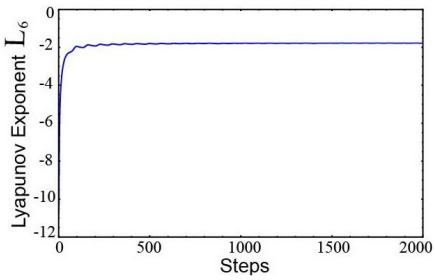

(f) Plot of the Lyapunov exponent L_6

Fig. 1 The convergence plot of the Lyapunov spectrum for the system (Eq. (2))

Table 1 A comparison of various chaotic systems with the new chaotic system

No.	System	Phase space dimension	KYD	A new chaotic system (Eq. (1))	
				Dimension	KYD
1	Lorenz [7]	3D	2.062	6D	2.202
2	Rossler [8]	3D	2.013	6D	2.202
3	Rikitake [9]	3D	2.0767	6D	2.202
4	Modified Lorentz [10]	3D	2.0984	6D	2.202
5	Rucklidge [14]	3D	2.0587	6D	2.202
6	Lu [15]	4D	3.0927	6D	2.202
7	Modified Lorentz [18]	4D	2.2211	6D	2.202
8	Modified Rikitake [21]	5D	4.0502	6D	2.202

2.3. Adaptive synchronization of the 6D novel hyperchaotic systems with unknown parameters

In this section, the adaptive control method is used to derive an adaptive feedback control law for globally synchronizing identical 6D novel hyperchaotic systems with unknown parameters. The system in Eq. (1) is written in the following form:

$$\begin{cases} x_1 = -x_1 + ax_2 - bx_4 - cx_5 \\ x_2 = -dx_2 + dx_1 - dx_1x_3 \\ x_3 = -ex_3 + dx_1x_2 \\ x_4 = -fx_4 + dx_1 \\ x_5 = -x_5 + gx_1 + bx_6 \\ x_6 = -fx_6 + hx_4 - dx_5 \end{cases} \tag{5}$$

In Eq. (7), unknown system parameters are determined as follows: $a = R$, $b = H$, $c = T$, $d = \mathrm{Pr}^{-1}$, $e = b\mathrm{Pr}^{-1}$, $f = Pm^{-1}$, $g = \sqrt{Ta}(1 + Ro)$, and $h = Ro\sqrt{Ta}$. The adaptive synchronization of identical 6D novel systems is considered with unknown system parameters. As the drive (or master) system, the system in Eq. (5) is taken; as the response (or slave) system, the following system is taken:

$$\begin{cases} y_1 = -y_1 + ay_2 - by_4 - cy_5 + u_1 \\ y_2 = -dy_2 + dy_1 - dy_1y_3 + u_2 \\ y_3 = -ey_3 + dy_1y_2 + u_3 \\ y_4 = -fy_4 + dy_1 + u_4 \\ y_5 = -y_5 + gy_1 + by_6 + u_5 \\ y_6 = -fy_6 + hy_4 - dy_5 + u_6 \end{cases} \tag{6}$$

where y_1, y_2, y_3, y_4, y_5, and y_6 are the states, and u_1, u_2, u_3, u_4, u_5, and u_6 are the controllers to be designed to achieve global chaos synchronization between the systems in Eqs. (5) and (6). The synchronization error between the identical chaotic systems is defined as $\xi_i(\tau) = y_i(t) - x_i(t)$ (i =1, 2, 3, 4, 5, and 6). The synchronization error dynamics is obtained as:

$$\begin{cases} \dot{\xi}_1 = -\xi_1 + a\xi_2 - b\xi_4 - c\xi_5 + u_1 \\ \dot{\xi}_2 = -d\xi_2 + d\xi_1 - d(y_1y_3 - x_1x_3) + u_2 \\ \dot{\xi}_3 = -e\xi_3 + d(y_1y_2 - x_1x_2) + u_3 \\ \dot{\xi}_4 = -f\xi_4 + d\xi_1 + u_4 \\ \dot{\xi}_5 = -\xi_5 + g\xi_1 + b\xi_6 + u_5 \\ \dot{\xi}_6 = -f\xi_6 + h\xi_4 - d\xi_5 + u_6 \end{cases} \tag{7}$$

The adaptive control law is written as follows:

$$\begin{cases} u_1 = \xi_1 - \hat{a}(t)\xi_2 + \hat{b}(t)\xi_4 + \hat{c}(t)\xi_5 - k_1\xi_1 \\ u_2 = \hat{d}(t)\xi_2 - \hat{d}(t)\xi_1 + \hat{d}(t)(y_1y_3 - x_1x_3) - k_2\xi_2 \\ u_3 = \hat{e}(t)\xi_3 - \hat{d}(t)(y_1y_2 - x_1x_2) - k_3\xi_3 \\ u_4 = \hat{f}(t)\xi_4 - \hat{d}(\tau)\xi_1 - k_4\xi_4 \\ u_5 = \xi_5 - \hat{g}(t)\xi_1 - \hat{b}(t)\xi_6 - k_5\xi_5 \\ u_6 = \hat{f}(t)\xi_6 - \hat{h}(t)\xi_4 + \hat{d}(t)\xi_5 - k_6\xi_6 \end{cases} \tag{8}$$

where k_1, k_2, k_3, k_4, k_5, and k_6 are positive constants controlling the synchronization speed. $\hat{a}(t)$, $\hat{b}(t)$, $\hat{c}(t)$, $\hat{d}(t)$, $\hat{e}(t)$, $\hat{f}(t)$, $\hat{g}(t)$, and $\hat{h}(t)$ are estimates of the unknown parameters a, b, c, d, e, f, g, and h respectively. The parameter estimation errors are defined by: $\xi_a(t) = a - \hat{a}(t)$, $\xi_b(t) = b - \hat{b}(t)$, $\xi_c(t) = c - \hat{c}(t)$, $\xi_d(t) = d - \hat{d}(t)$, $\xi_e(t) = e - \hat{e}(t)$, $\xi_f(t) = f - \hat{f}(t)$, $\xi_g(t) = g - \hat{g}(t)$, and $\xi_h(t) = h - \hat{h}(t)$. By substituting Eq. (8) into the error dynamics (Eq. (7)), the following system is obtained:

$$\begin{cases} \dot{\xi}_1 = \xi_a\xi_2 - \xi_b\xi_4 - \xi_c\xi_5 - k_1\xi_1 \\ \dot{\xi}_2 = -\xi_d\xi_2 + \xi_d\xi_1 - \xi_d(y_1y_3 - x_1x_3) - k_2\xi_2 \\ \dot{\xi}_3 = -\xi_e\xi_3 + \xi_d(y_1y_2 - x_1x_2) - k_3\xi_3 \\ \dot{\xi}_4 = -\xi_f\xi_4 + \xi_d\xi_1 - k_4\xi_4 \\ \dot{\xi}_5 = \xi_g\xi_1 + \xi_b\xi_6 - k_5\xi_5 \\ \dot{\xi}_6 = -\xi_f\xi_6 + \xi_h\xi_4 - \xi_d\xi_5 - k_6\xi_6 \end{cases} \tag{9}$$

Next, the considered quadratic Lyapunov function can be defined by:

$$\Lambda = \frac{1}{2}\left(\sum_{\alpha}\xi_{\alpha}^2 + \sum_{\beta}\xi_{\beta}^2\right);\ \alpha = 1,\ 2,\ 3,\ 4,\ 5,\ 6;\ \beta = a,\ b,\ c,\ d,\ e,\ f,\ g,\ h \tag{10}$$

Eq. (11) is found by taking into account the values of $\dot{\xi}_a(t) = -\dot{\hat{a}}(t)$, $\dot{\xi}_b(t) = -\dot{\hat{b}}(t)$, $\dot{\xi}_c(t) = -\dot{\hat{c}}(t)$, $\dot{\xi}_d(t) = -\dot{\hat{d}}(t)$, $\dot{\xi}_e(t) = -\dot{\hat{e}}(t)$, $\dot{\xi}_f(t) = -\dot{\hat{f}}(t)$, $\dot{\xi}_g(t) = -\dot{\hat{g}}(t)$, $\dot{\xi}_h(t) = -\dot{\hat{h}}(t)$, as well as the value of Eq. (10).

$$\frac{d\Lambda}{dt} = -k_1^2\xi_1^2 - k_1^2\xi_2^2 - k_3^2\xi_3^2 - k_4^2\xi_4^2 - k_5^2\xi_5^2 - k_6^2\xi_6^2 + \xi_a(\xi_1\xi_2 - \dot{\hat{a}}) + \xi_b(-\xi_1\xi_4 - \dot{\hat{b}}) + \xi_c(-\xi_1\xi_5 - \dot{\hat{c}}) +$$
$$\xi_d(-\xi_2^2 + \xi_1(\xi_2 + \xi_4) - \xi_2(y_1y_3 - x_1x_3) + \xi_3(y_1y_2 - x_1x_2) - \xi_5\xi_6 - \dot{\hat{d}}) + \xi_e(-\xi_3^2 - \dot{\hat{e}}) + \quad (11)$$
$$\xi_f(-\xi_4^2 - \xi_6^2 - \dot{\hat{f}}) + \xi_g(\xi_1\xi_5 - \dot{\hat{g}}) + \xi_h(\xi_4\xi_6 - \dot{\hat{h}})$$

From Eq. (11), the parameter update law is obtained as follows: $\dot{\hat{a}} = \xi_1\xi_2$, $\dot{\hat{b}} = -\xi_1\xi_4$, $\dot{\hat{c}} = -\xi_1\xi_5$, $\dot{\hat{d}} = -\xi_2^2 + \xi_1(\xi_2 + \xi_4) - \xi_2(y_1y_3 - x_1x_3) + \xi_3(y_1y_2 - x_1x_2) - \xi_5\xi_6$, $\dot{\hat{e}} = -\xi_3^2$, $\dot{\hat{f}} = -\xi_4^2 - \xi_6^2$, $\dot{\hat{g}} = \xi_1\xi_5$, and $\dot{\hat{h}} = \xi_4\xi_6$. Following the work of Vaidyanathan et al. [20], the main result of this section is presented and proven.

Theorem: The identical novel 6D hyperchaotic systems in Eqs. (5) and (6) with unknown system parameters are globally and exponentially synchronized for all initial conditions by the adaptive control law (Eq. (8)) and the parameter update law, where k_1, k_2, k_3, k_4, k_5, and k_6 are positive gain constants.

Proof: According to the Lyapunov stability theory, it follows that if Λ is a positive definite function and $d\Lambda/dt$ is a negative semidefinite function, then the system is consistent and stable at the origin of the equilibrium state. By substituting the parameter update law into Eq. (11), the time derivative of Λ is obtained as:

$$\frac{d\Lambda}{dt} = -k_1^2\xi_1^2 - k_1^2\xi_2^2 - k_3^2\xi_3^2 - k_4^2\xi_4^2 - k_5^2\xi_5^2 - k_6^2\xi_6^2 \quad (12)$$

which is a negative semi-definite function on $\Re^6$. The synchronization error $\xi(t)$ and the parameter estimation error are globally bounded. From Eq. (12) outlined above, Eq. (13) is inferred. Furthermore, by integrating the inequality (Eq. (13)) from 0 to t, Eq. (14) is obtained:

$$k\|\xi(t)\|^2 \leq -\frac{d\Lambda}{dt} \quad (13)$$

$$k\int_0^t \|\xi(\tau)\|^2 d\tau \leq \Lambda(0) - \Lambda(t) \quad (14)$$

where $k = \min\{k_1, k_2, k_3, k_4, k_5, k_6\}$. Using Barbalat's lemma [20], it can be concluded that $\xi(t) \longrightarrow 0$ exponentially as $t \longrightarrow \infty$ for all initial conditions $\xi(0) \in \Re^6$. Thus, the active synchronization error system (Eq. (7)) is asymptotically stable at the origin and the synchronization is effectively realized. This completes the proof.

For numerical simulations, the parameter values of the novel drive system (Eq. (5)) and the novel response system (Eq. (6)) is taken as in the chaotic case: $a = 58$, $b = 2$, $c = 0.1$, $d = 0.1$, $e = 8/30$, $f = 1$, $g = 8.21$, and $h = -24.65$. The gain constants are taken as $k_i = 10$ for $i = 1, 2, \ldots\ldots, 6$. The initial conditions of the drive system (Eq. (5)) are taking $x_1(0) = x_2(0) = x_3(0) = x_4(0) = x_5(0) = x_6(0) = 1$.

The initial values of the response system (Eq. (6)) are chosen as $y_1(0) = y_2(0) = y_3(0) = y_4(0) = y_5(0) = y_6(0) = 15$. Also, the initial conditions of the parameter can be estimated as follows: $\hat{a}(t) = 59$, $\hat{b}(t) = 2.5$, $\hat{c}(t) = 0.15$, $\hat{d}(t) = 0.9$, $\hat{e}(t) = 0.3$, $\hat{f}(t) = 0.9$, $\hat{g}(t) = 8.25$, and $\hat{h}(t) = -25$. The timing diagrams of $x_1 - y_1$, $x_2 - y_2$, $x_3 - y_3$, $x_4 - y_4$, $x_5 - y_5$, and $x_6 - y_6$ are shown in Fig. 2 and Fig. 3. Fig. 4 shows the convergence of the synchronization errors ξ_1, ξ_2, ξ_3, ξ_4, ξ_5, and ξ_6 to zero exponentially with time.

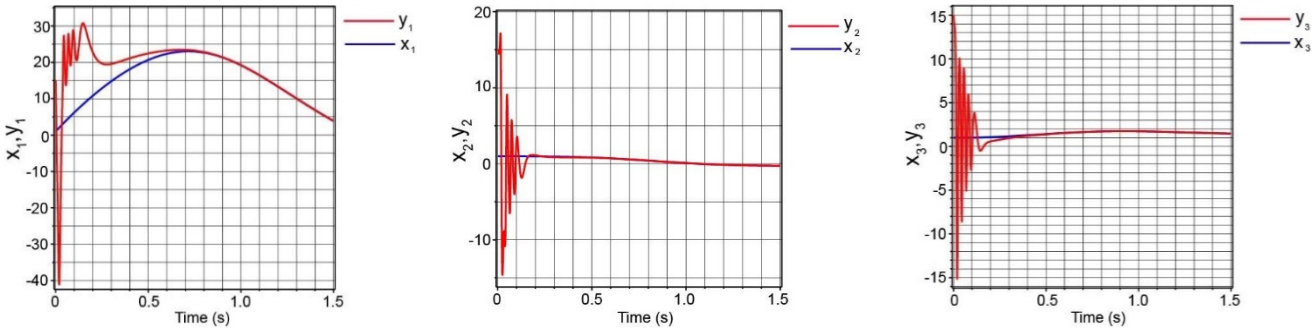

(a) $x_1 - y_1$ (b) $x_2 - y_2$ (c) $x_3 - y_3$

Fig. 2 Synchronization of the states $x_1 - y_1$, $x_2 - y_2$, and $x_3 - y_3$ of the chaotic systems

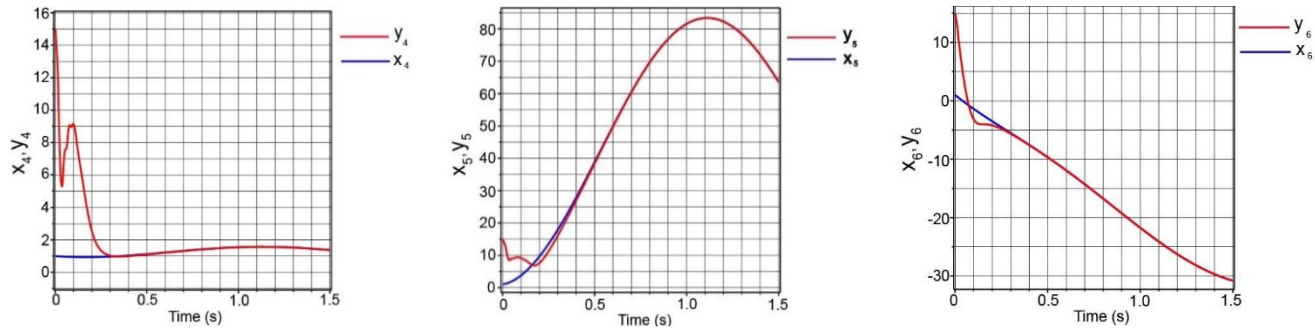

(a) $x_4 - y_4$ (b) $x_5 - y_5$ (c) $x_6 - y_6$

Fig. 3 Synchronization of the states $x_4 - y_4$, $x_5 - y_5$, and $x_6 - y_6$ of the chaotic systems

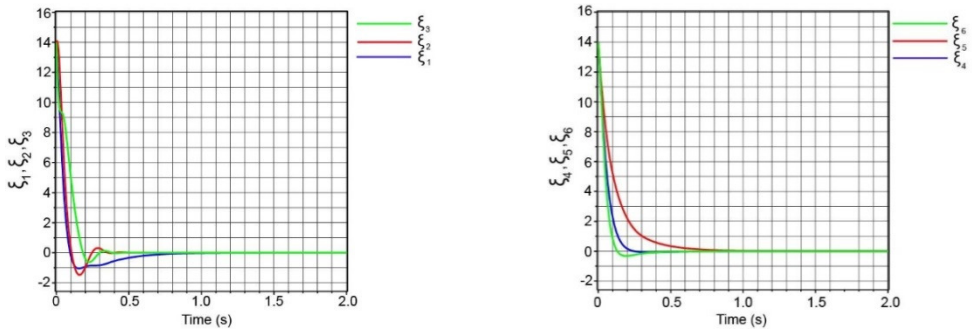

(a) ξ_1, ξ_2, ξ_3 (b) ξ_4, ξ_5, ξ_6

Fig. 4 Time-history of the synchronization errors

2.4. *Matlab-Simulink model*

For the system of differential equations (Eq. (2)), a Matlab-Simulink model based on the implementation of six integrators is constructed:

$$\begin{cases} x_1 = \int(-x_1 + Rx_2 - 2x_4 - 0.1x_5)d\tilde{t} \\ x_2 = \dfrac{1}{10}\int\left(-x_2 + x_1 - x_1x_3\right)d\tilde{t} \\ x_3 = \dfrac{1}{10}\int\left(-\dfrac{8}{3}x_3 + x_1x_2\right)d\tilde{t} \\ x_4 = \int(-x_4 + \dfrac{1}{10}x_1)d\tilde{t} \\ x_5 = \int(-x_5 + 8.21x_1 + 2x_6)d\tilde{t} \\ x_6 = \int(-x_6 - 24.65x_4 - \dfrac{1}{10}x_5)d\tilde{t} \end{cases} \tag{15}$$

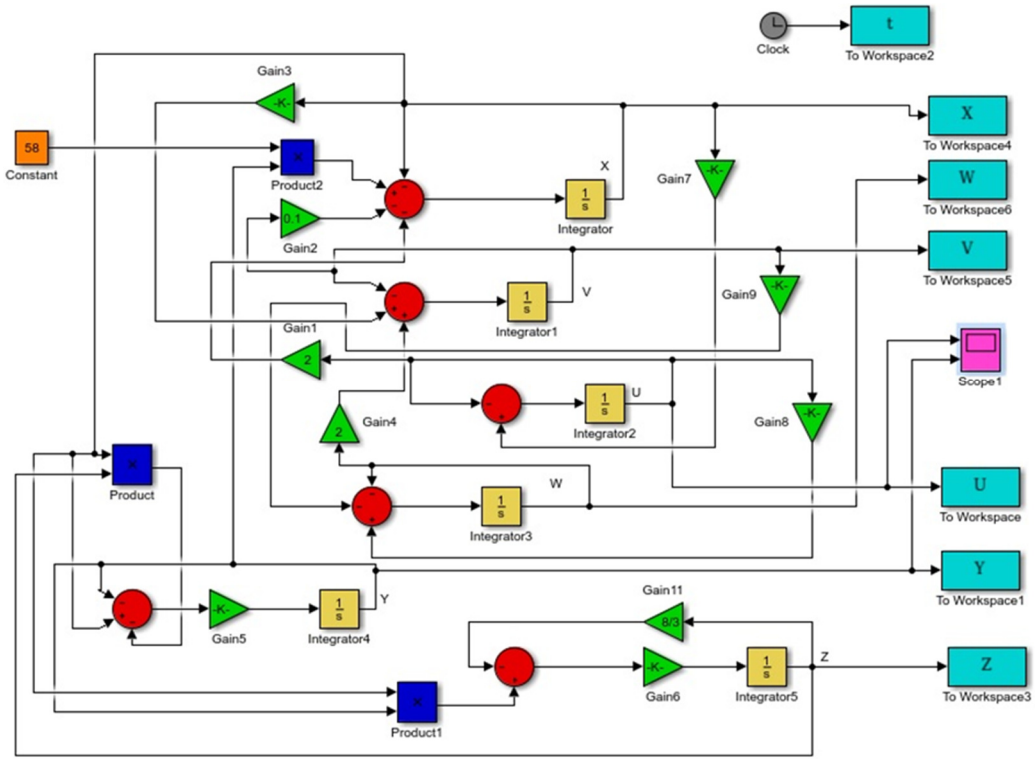

Fig. 5 The Matlab-Simulink model for Eq. (2)

Fig. 5 shows a diagram of the Matlab-Simulink model, which consists of interconnected amplification blocks, summation and subtraction, multiplication, integration, and signal recording devices. Simulation data is displayed using the Workspace blocks. Fig. 6 and Fig. 7 show the results of modeling the equations system (Eq. (2) or (15)) for the parameter $R = 58$. On the phase portraits of Fig. 6, one can see the complexity of trajectories, which is the characteristic of strange attractors. Temporal distributions of the coordinates' values ($x_1(\tilde{t}) = X, x_2(\tilde{t}) = Y, x_3(\tilde{t}) = Z, x_4(\tilde{t}) = U, x_5(\tilde{t}) = V$, and $x_6(\tilde{t}) = W$) also have a complex structure characteristic of chaotic signals (Fig. 7).

Note that a direct implementation of Eq. (2) with an electronic circuit presents one certain difficulty. The dynamic variables in Eq. (2) occupy a wide dynamic range with values that exceed reasonable power supply limits. The operating voltage range of operational amplifiers is typically -15 V to +15 V in practical electronic circuits. In the work of Pecora and Carroll [29], this problem was proposed to be eliminated by a simple variable of the dynamic system transformation. For the current case, it is necessary to rescale the following variables: $x_1 = 10X_1$, $x_5 = 20X_5$, and $x_6 = 10X_6$. The rest of variables $x_2 = X_2$, $x_3 = X_3$, and $x_4 = X_4$ are simply redesignated. With this scaling, Eq. (3) is transformed to the following form:

$$\begin{cases} \dot{X}_1 = -X_1 + 5.8X_2 - 0.2X_4 - 0.2X_5 \\ \dot{X}_2 = -0.1X_2 + X_1 - X_1X_3 \\ \dot{X}_3 = -\dfrac{8}{30}X_3 + X_1X_2 \\ \dot{X}_4 = -X_4 + X_1 \\ \dot{X}_5 = -X_5 + 4.12X_1 + X_6 \\ \dot{X}_6 = -X_6 - 2.465X_4 - 0.2X_5 \end{cases} \tag{16}$$

Note that the two systems in Eqs. (2) and (16) are equivalent since the linear transformation does not change the physical properties of nonlinear systems. The chaotic solutions of Eq. (16) obtained using the Matlab-Simulink model are shown in Fig. 8. From the figure, it can be seen that the range of dynamic variables' values has significantly decreased compared to the dynamic variables' values on the graphs of chaotic solutions.

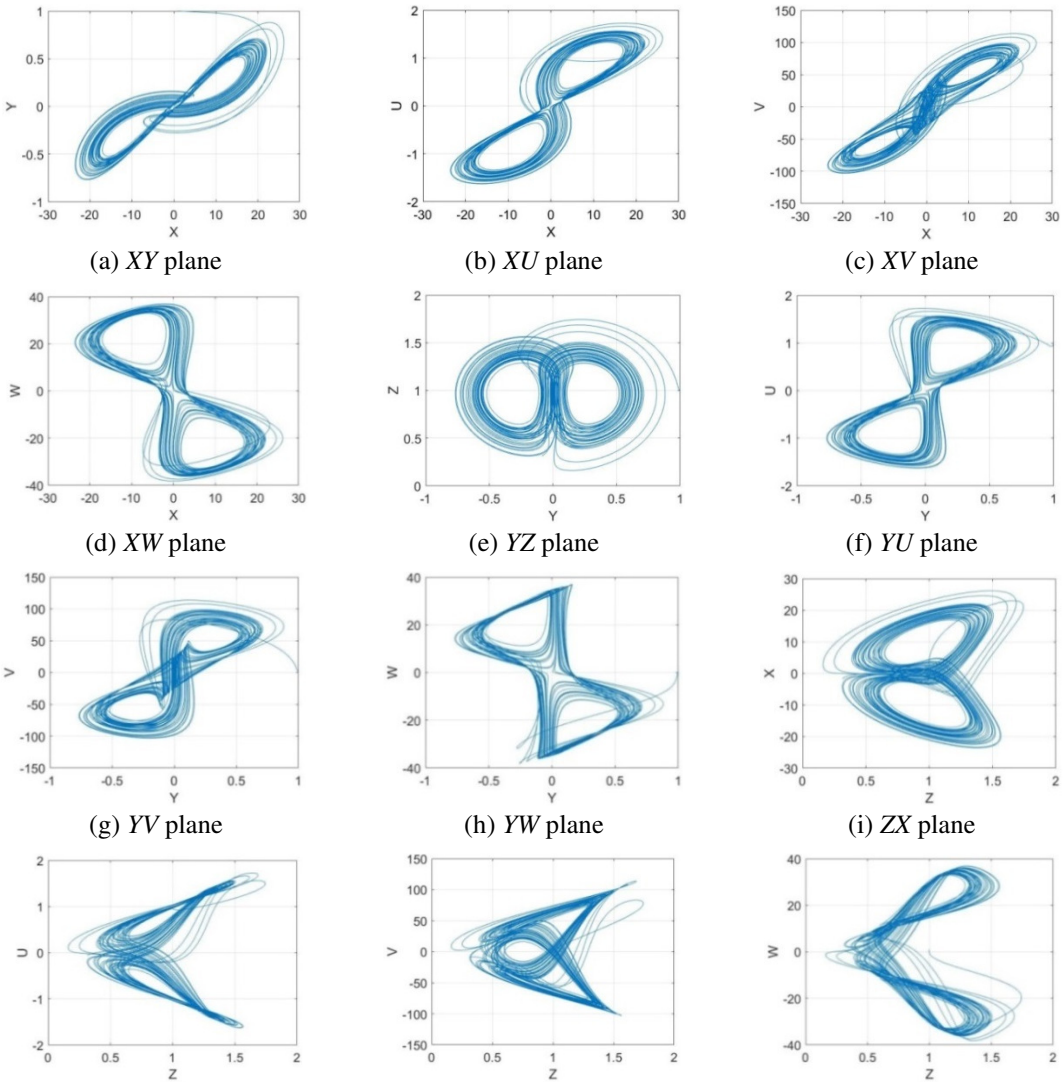

(a) *XY* plane (b) *XU* plane (c) *XV* plane

(d) *XW* plane (e) *YZ* plane (f) *YU* plane

(g) *YV* plane (h) *YW* plane (i) *ZX* plane

(j) *ZU* plane (k) *ZV* plane (l) *ZW* plane

Fig. 6 Phase portraits in different planes

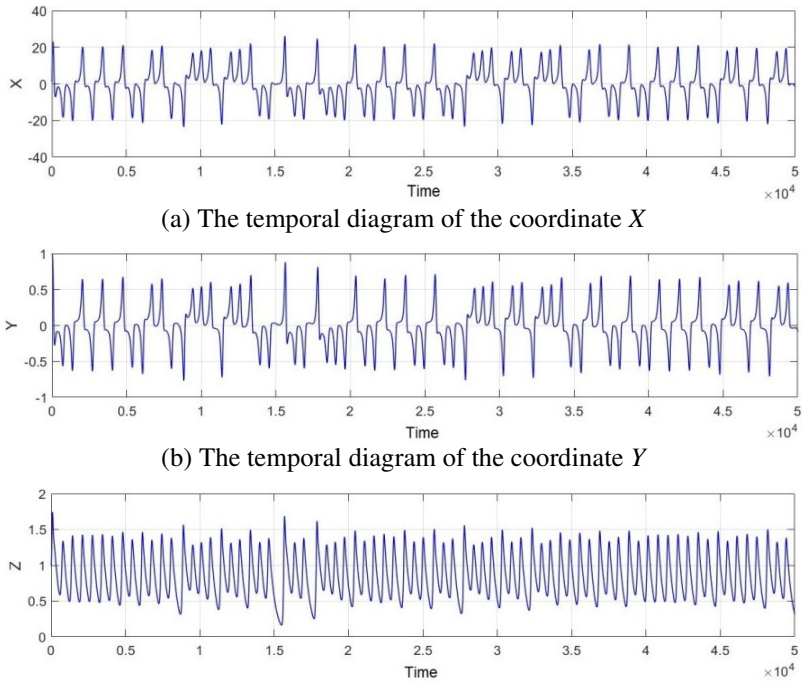

(a) The temporal diagram of the coordinate *X*

(b) The temporal diagram of the coordinate *Y*

(c) The temporal diagram of the coordinate *Z*

Fig. 7 Temporal diagrams of the values of different coordinates

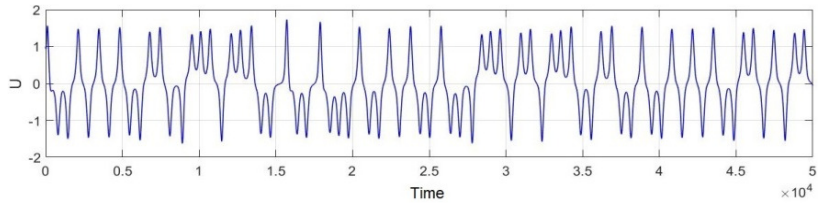

(d) The temporal diagram of the coordinate *U*

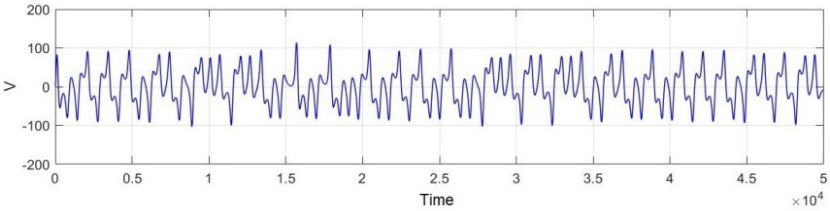

(e) The temporal diagram of the coordinate *V*

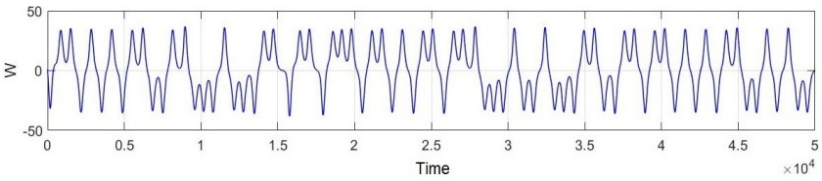

(f) The temporal diagram of the coordinate *W*

Fig. 7 Temporal diagrams of the values of different coordinates (continued)

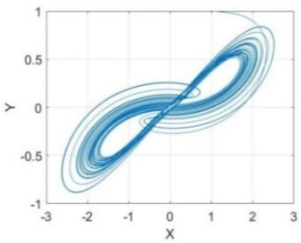

(a) *XY* plane

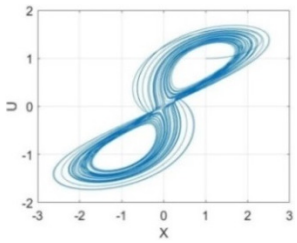

(b) *XU* plane

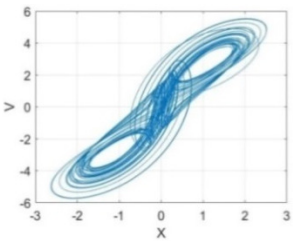

(c) *XV* plane

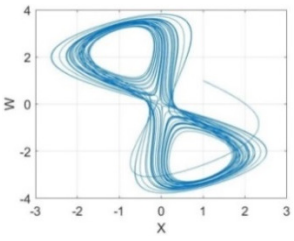

(d) *XW* plane

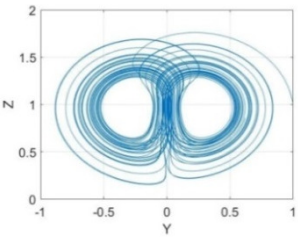

(e) *YZ* plane

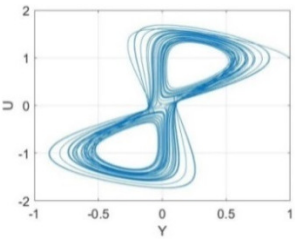

(f) *YU* plane

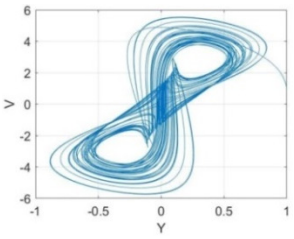

(g) *YV* plane

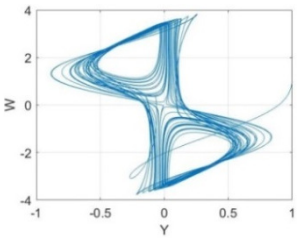

(h) *YW* plane

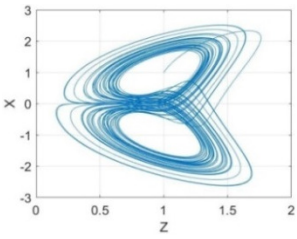

(i) *ZX* plane

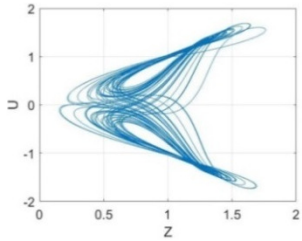

(j) *ZU* plane

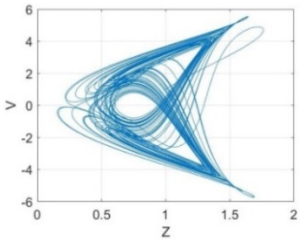

(k) *ZV* plane

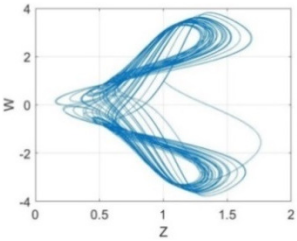

(l) *ZW* plane

Fig. 8 The chaotic attractors of the modified chaotic system (Eq. (16))

2.5. LabVIEW model

Of great interest is the modeling of nonlinear dynamic systems using various software environments, which makes it possible to demonstrate various informational properties of chaotic oscillations. To simulate a chaotic system (Eq. (16)) and demonstrate the results, the LabVIEW software environment is used. LabVIEW is a graphical software platform that is now very widely used in engineering applications [30]. For the development of algorithms in LabVIEW, a visual platform has been created. Fig. 9 shows a block diagram of the chaotic system (Eq. (16)). This model is created using Control & Simulation toolbox in LabVIEW. As can be seen from Fig. 9, for modeling differential equations (Eq. (16)), operations of addition, multiplication, multiplication on a fixed number, and integration are used. Fig. 10 shows a programming interface that displays these properties of information modeling in the form of phase portraits in the planes X_1X_2, X_2X_5, X_2X_3, X_3X_4, X_3X_5, and X_1X_6 for the initial conditions $X_1(0) = X_2(0) = X_3(0) = X_4(0) = X_5(0) = X_6(0) = 1$. Comparing phase portraits in Fig. 8 and Fig. 10, it can be seen that the results of modeling in Matlab-Simulink and LabVIEW the chaotic system (Eq. (16)) coincide.

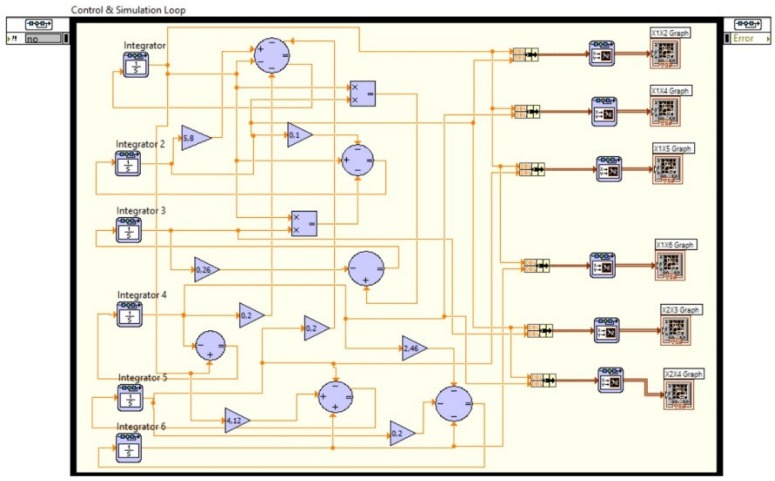

Fig. 9 The block diagram that implements a chaotic system (Eq. (16)) in LabVIEW

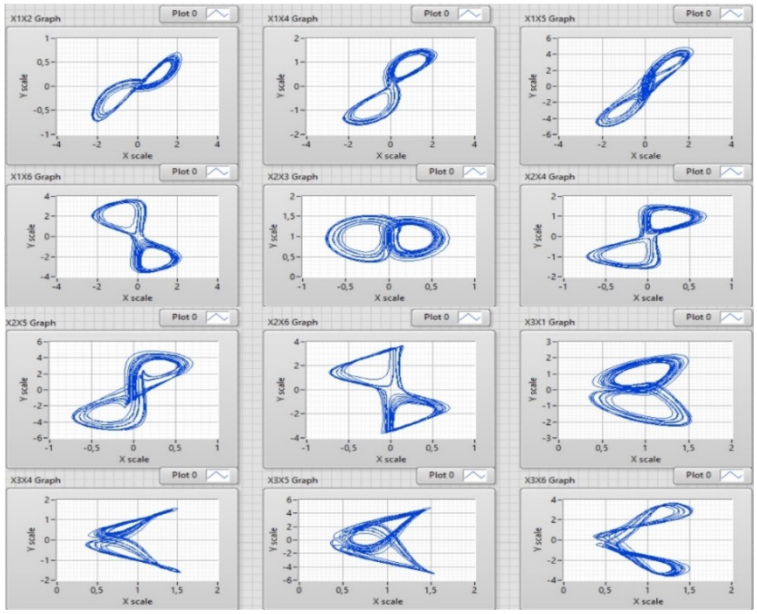

Fig. 10 Phase portraits simulated in LabVIEW

3. An Implementation of Chaotic Circuits with MultiSim

The circuit implementation of chaotic systems is an important task in engineering applications such as secure communication and random bits generation. It is obvious that the simple circuit implementation of the dynamic equations system (Eq. (16)) will be composed of six operational amplifiers performing the signal integration function. Dynamic system

variables are represented by appropriate electrical signals that correspond to instantaneous voltage values $U_1(\tau)$, $U_2(\tau)$, $U_3(\tau)$, $U_4(\tau)$, $U_5(\tau)$, and $U_6(\tau)$ on capacitors C_1, C_2, C_3, C_4, C_5, and C_6. In accordance with the laws of Kirchhoff for electrical circuits, the electrical analog of the system (Eq. (17)) takes the following form:

$$\begin{cases} C_1\dfrac{dU_1}{d\tau} = -\dfrac{U_1}{R_{11}} + \dfrac{U_2}{R_{12}} - \dfrac{U_4}{R_{13}} - \dfrac{U_5}{R_{14}} \\ C_2\dfrac{dU_2}{d\tau} = -\dfrac{U_2}{R_{21}} + \dfrac{U_1}{R_{22}} - \dfrac{U_1U_3}{R_{23}K} \\ C_3\dfrac{dU_3}{d\tau} = -\dfrac{U_3}{R_{31}} + \dfrac{U_1U_2}{R_{32}K} \\ C_4\dfrac{dU_4}{d\tau} = -\dfrac{U_4}{R_{41}} + \dfrac{U_1}{R_{42}} \\ C_5\dfrac{dU_5}{d\tau} = -\dfrac{U_5}{R_{51}} + \dfrac{U_1}{R_{52}} + \dfrac{U_6}{R_{53}} \\ C_6\dfrac{dU_6}{d\tau} = -\dfrac{U_6}{R_{61}} - \dfrac{U_4}{R_{62}} - \dfrac{U_5}{R_{63}} \end{cases} \tag{17}$$

where R_{ij} are resistors $(i, j) =$ 1, 2, 3, 4, 5, 6; K is a scaling coefficient for the multiplier. The normalized resistor is chosen as $R_0 = 10$ kΩ and the normalized capacitor is chosen as $C_0 = 100$ nF. Then, the time constant is equal to $t_0 = R_0C_0 = 10^{-3}$ s. The state variables of the system in Eq. (18) are rescaled as follows: $U_1 = U_0\tilde{X}_1$, $U_2 = U_0\tilde{X}_2$, $U_3 = U_0\tilde{X}_3$, $U_4 = U_0\tilde{X}_4$, $U_5 = U_0\tilde{X}_5$, $U_6 = U_0\tilde{X}_6$, $K = U_0K'$, and $\tau = t_0t$. Hence, Eq. (18) is written in a dimensionless form:

$$\begin{cases} \dfrac{C_1}{C_0}\dfrac{d\tilde{X}_1}{dt} = -\dfrac{R_0}{R_{11}}\tilde{X}_1 + \dfrac{R_0}{R_{12}}\tilde{X}_2 - \dfrac{R_0}{R_{13}}\tilde{X}_4 - \dfrac{R_0}{R_{14}}\tilde{X}_5 \\ \dfrac{C_2}{C_0}\dfrac{d\tilde{X}_2}{dt} = -\dfrac{R_0}{R_{21}}\tilde{X}_2 + \dfrac{R_0}{R_{22}}\tilde{X}_1 - \dfrac{R_0}{R_{23}K'}\tilde{X}_1\tilde{X}_3 \\ \dfrac{C_3}{C_0}\dfrac{d\tilde{X}_3}{dt} = -\dfrac{R_0}{R_{31}}\tilde{X}_3 + \dfrac{R_0}{R_{32}K'}\tilde{X}_1\tilde{X}_2 \\ \dfrac{C_4}{C_0}\dfrac{d\tilde{X}_4}{dt} = -\dfrac{R_0}{R_{41}}\tilde{X}_4 + \dfrac{R_0}{R_{42}}\tilde{X}_1 \\ \dfrac{C_5}{C_0}\dfrac{d\tilde{X}_5}{dt} = -\dfrac{R_0}{R_{51}}\tilde{X}_5 + \dfrac{R_0}{R_{52}}\tilde{X}_1 + \dfrac{R_0}{R_{53}}\tilde{X}_6 \\ \dfrac{C_6}{C_0}\dfrac{d\tilde{X}_6}{dt} = -\dfrac{R_0}{R_{61}}\tilde{X}_6 - \dfrac{R_0}{R_{62}}\tilde{X}_4 - \dfrac{R_0}{R_{63}}\tilde{X}_5 \end{cases} \tag{18}$$

By substituting $R_0 = 10$ kΩ, $C_1 = C_2 = C_3 = C_4 = C_5 = C_6 = C_0 = 100$ nF, and $K' = 10$ into Eq. (18) and comparing numerical values before the output voltages of the systems in Eq. (16), the value of electronic circuit resistors is obtained:

$$\begin{cases} \dfrac{d\tilde{X}_1}{dt} = -\dfrac{10\text{k}}{10\text{k}}\tilde{X}_1 + \dfrac{10\text{k}}{1.724\text{k}}\tilde{X}_2 - \dfrac{10\text{k}}{50\text{k}}\tilde{X}_4 - \dfrac{10\text{k}}{50\text{k}}\tilde{X}_5 \\ \dfrac{d\tilde{X}_2}{dt} = -\dfrac{10\text{k}}{100\text{k}}\tilde{X}_2 + \dfrac{10\text{k}}{10\text{k}}\tilde{X}_1 - \dfrac{10\text{k}}{1\text{k}\cdot 10}\tilde{X}_1\tilde{X}_3 \\ \dfrac{d\tilde{X}_3}{dt} = -\dfrac{10\text{k}}{37.5\text{k}}\tilde{X}_3 + \dfrac{10\text{k}}{1\text{k}\cdot 10}\tilde{X}_1\tilde{X}_2 \\ \dfrac{d\tilde{X}_4}{dt} = -\dfrac{10\text{k}}{10\text{k}}\tilde{X}_4 + \dfrac{10\text{k}}{10\text{k}}\tilde{X}_1 \\ \dfrac{d\tilde{X}_5}{dt} = -\dfrac{10\text{k}}{10\text{k}}\tilde{X}_5 + \dfrac{10\text{k}}{2.43\text{k}}\tilde{X}_1 + \dfrac{10\text{k}}{10\text{k}}\tilde{X}_6 \\ \dfrac{d\tilde{X}_6}{dt} = -\dfrac{10\text{k}}{10\text{k}}\tilde{X}_6 - \dfrac{10\text{k}}{4.056\text{k}}\tilde{X}_4 - \dfrac{10\text{k}}{50\text{k}}\tilde{X}_5 \end{cases} \tag{19}$$

The analog circuit of the system in Eq. (19) is designed in a MultiSim environment and presented in Fig. 11. For convenience, the subsystem SC1 is used for the first three equations (Eq. (19)). The electronic circuit of the subsystem is shown in Fig. 12**.** From Fig. 11 and Fig. 12, it can be seen that the circuits are obtained on the basis of operational amplifiers TL084ACN and analog multipliers A1 and A2 (e.g., AD633 series). Terminals IO1, IO2, IO3, IO4, IO5, and IO6 on the diagram (Fig. 11) correspond to signal outputs $\tilde{X}_1$, $\tilde{X}_2$, $\tilde{X}_3$, $\tilde{X}_4$, $\tilde{X}_5$, and $\tilde{X}_6$. By connecting a dual-channel oscilloscope to different outputs, different phase portraits in the MultiSim environment are obtained, which are shown in Fig. 13. From the MultiSim outputs in Fig. 13, Matlab-Simulink in Fig. 8, and LabVIEW in Fig. 10, it can be noted that the results are similar.

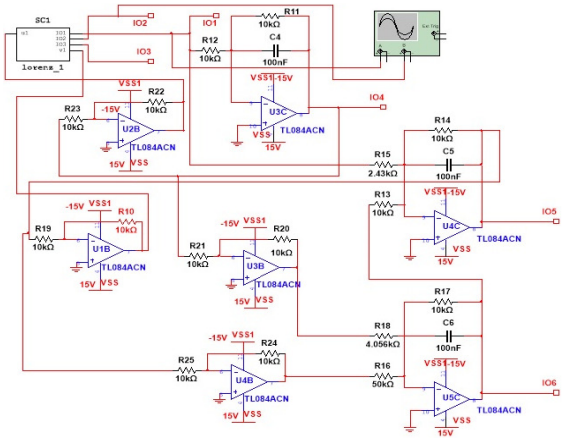

Fig. 11 The electronic circuit of the chaotic oscillation generator based on the equation system (Eq. (19))

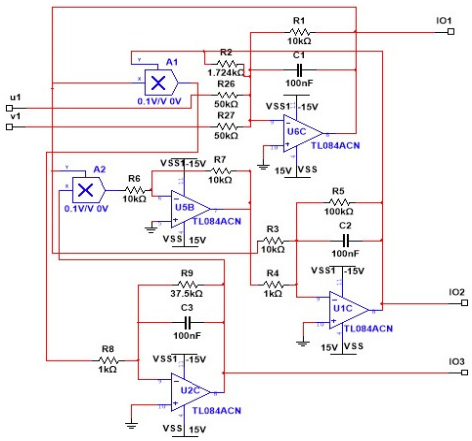

Fig. 12 The electronic circuit of the subsystem SC1

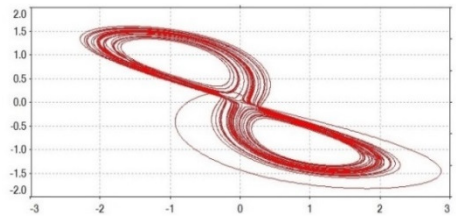

(a) $\tilde{X}_1\tilde{X}_2$

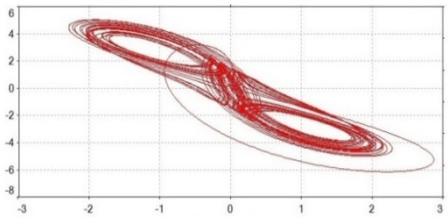

(b) $\tilde{X}_1\tilde{X}_4$

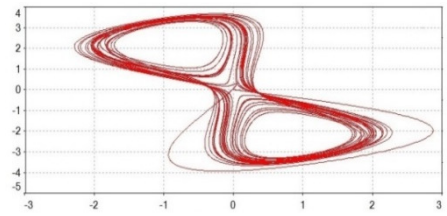

(c) $\tilde{X}_1\tilde{X}_5$

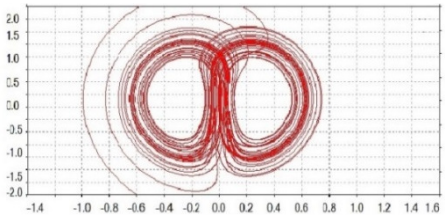

(d) $\tilde{X}_1\tilde{X}_6$

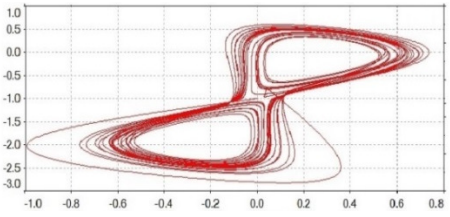

(e) $\tilde{X}_2\tilde{X}_3$

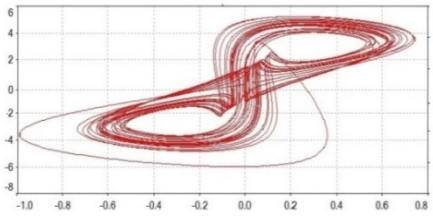

(f) $\tilde{X}_2\tilde{X}_4$

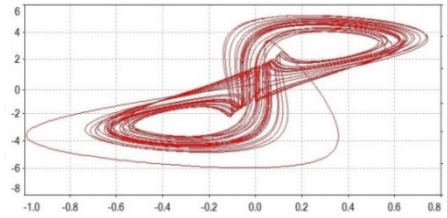

(g) $\tilde{X}_2\tilde{X}_5$

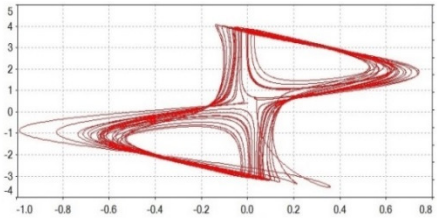

(h) $\tilde{X}_2\tilde{X}_6$

Fig. 13 Chaotic phase trajectories displayed in MultiSim oscilloscopes

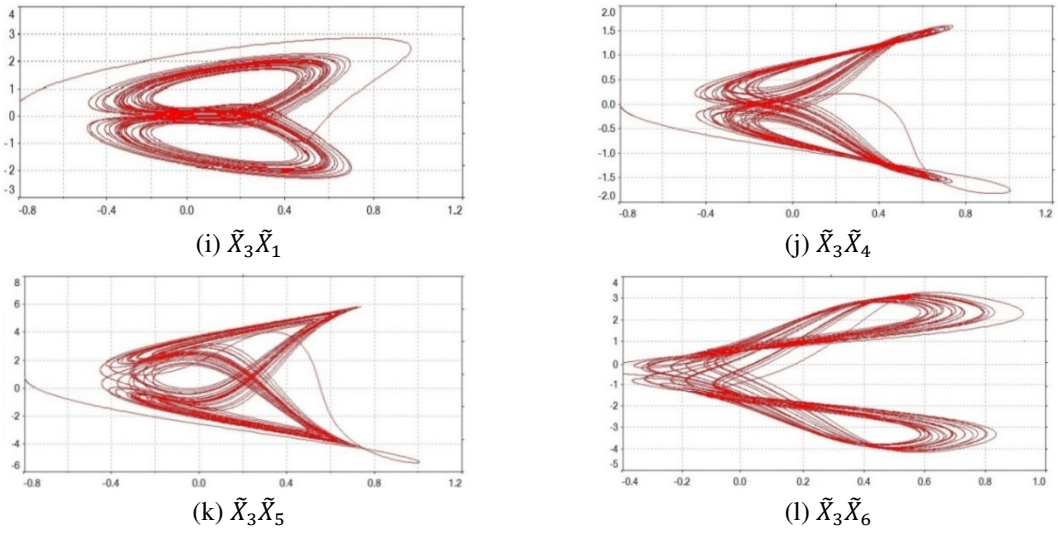

(i) $\tilde{X}_3\tilde{X}_1$ (j) $\tilde{X}_3\tilde{X}_4$

(k) $\tilde{X}_3\tilde{X}_5$ (l) $\tilde{X}_3\tilde{X}_6$

Fig. 13 Chaotic phase trajectories displayed in Multisim oscilloscopes (continued)

4. Simulation of Chaotic Masking and Signal Decoding in MultiSim

Fig. 14 shows a block diagram of a simple way of hiding information using a chaotic system (Eq. (3)) [29]. From this block diagram, it can be seen that the information signal S (e.g., a sinusoidal form) is additively mixed with the chaotic signal X_1 in the adder block (chaotic transmitter) and then transmitted to the receiving device (chaotic receiver). The transmitting signal M can be mathematically represented as the sum of the signals S and X_1: $M = S + X_1$. Synchronization of the communication system is carried out by establishing the same dynamic operation modes of the transmitting $D(X_1, \ldots\ldots, X_6)$ and receiving $R(X_{1r}, \ldots\ldots, X_{6r})$ parts of the communication system using the transmitted signal X_1 generated by the receiving side. In the receiving part, the chaotic signal is synchronized with the chaotic signal X_{1r}, and then the information signal is detected by subtracting the synchronous response X_{1r} from the received signal M. As a result, a new signal S_r is obtained at the output. The difference between S and S_r represents the error of communication channel $E = S - S_r$.

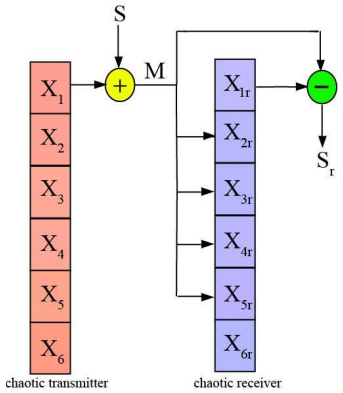

Fig. 14 The block diagram for chaotic secure communication

4.1. Multisim simulation of the chaotic secure communication scheme

Following the work of Xiong et al. [18], a scheme for chaotic modulation secure communication based on chaotic synchronization of a new 6D chaotic generator is considered. The circuit for chaotic masking and signal decoding is designed in the Multisim environment, which is shown in Fig. 15.

The left side of the diagram represents the transmitting (transmitter) system, and the right side represents the receiving system (receiver). The transmitting part consists of a chaos generator GS1, a periodic signal generator GS (frequency 1 kHz, amplitude 1 V), and a modulator. The electronic circuit of the chaos generator GS1 is shown in Fig. 11 and is realized into an

insular block for convenience. A similar chaos generator block GS2 is contained in the receiving part, which has identical characteristics to the GS1 block. The modulator performs the function of signal superposition, which is carried out using an inverting adder (U1B) and an inverter (U2B). The signal from the modulator is transmitted to the receiving system via a communication channel (wired or wireless). The operational amplifier (U3B) of the receiving system is made in the form of a demodulator, which consists of a single-phase adder. Its input is a modulated chaotic signal and a chaotic signal from the GS2 generator. At the output, a signal is obtained from the difference between two chaotic signals. Further, this signal is inverted by the operational amplifier (U4B) and an information signal is obtained at the output, thus completing the chaotic secure communication.

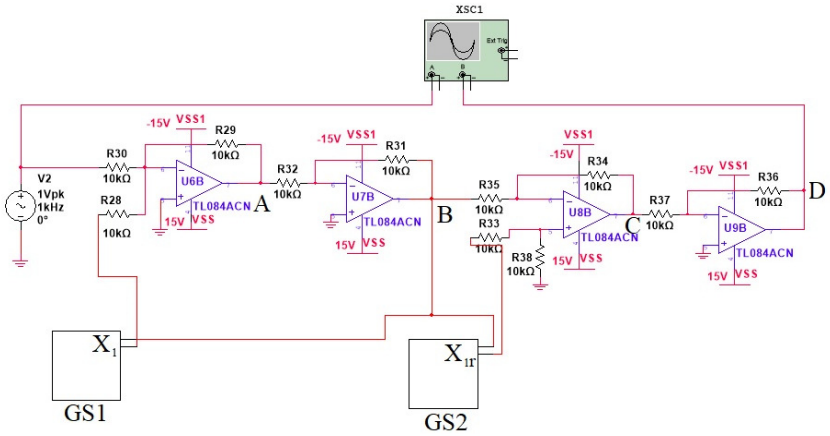

Fig. 15 The electronic circuit for the secure transmission of information with chaotic masking

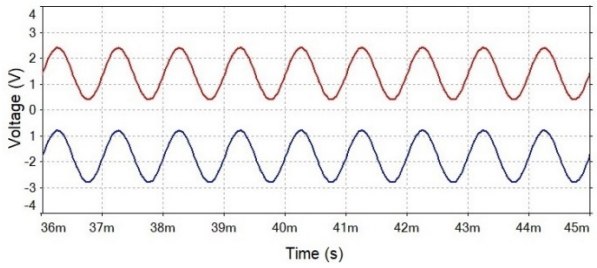

(a) The transmitting and receiving waveform

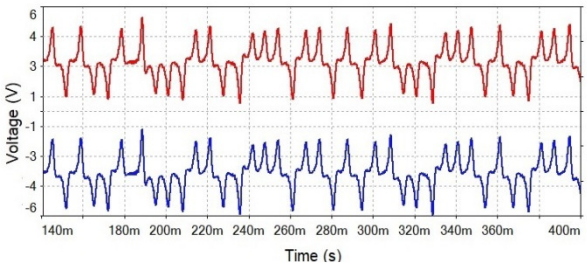

(b) Chaotic signals generated by generators GS1 and GS2

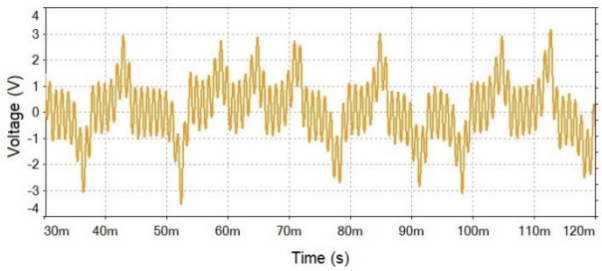

(c) The mixed chaotic signal

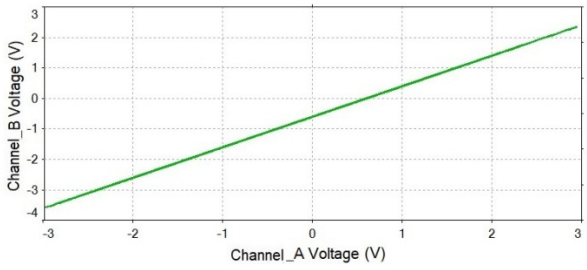

(d) The synchronous phase diagram

Fig. 16 MultiSim simulation outputs from the XSC1 oscilloscope

The whole process of the proposed chaotic secure communication can be expressed as follows: $S(\tau)$ is a transmitted signal and $X(\tau)$ is a chaotic signal. Then, at point **A**, after the operational amplifier U1B in Fig. 15, an additive (mixed) signal $M_A(\tau)$ is obtained, which is described as:

$$M_A(\tau) = S(\tau) + X(\tau) \tag{20}$$

At point **B**, after the operational amplifier U2B, the output from the inverting adder of the modulation circuit is obtained:

$$M_B(\tau) = -M_A(\tau) = -S(\tau) - X(\tau) \tag{21}$$

Further, the signal enters the demodulator, which consists of a single-phase adder (operational amplifier U3B) and an inverter (operational amplifier U4B). After the operational amplifier U3B at point **C**, the signal consists of the sum of the inverted signal M_B and the synchronous signal X_r from the receiving generator GS2:

$$M_C(\tau) = M_B(\tau) + X_r(\tau) = -S(\tau) - X(\tau) + X_r(\tau) \Rightarrow -S(\tau) \tag{22}$$

After the inverter U4B at point **D**, the information signal $M_D(\tau) = M_C(\tau) = \mathrm{S}(\tau)$ is received. Therefore, the receiving system maintains synchronization with the transmitting system more easily $|X_r - \mathrm{X}|_{r\to\infty} \longrightarrow 0$, and the more reliable secure transmission of information is maintained.

The simulation results of the electronic circuit for chaotic masking in MultiSim are shown in Fig. 16. Using the XSC1 oscilloscope, the temporal diagrams of the input information signal (a sine wave with the amplitude of 1 V and the frequency of 1 kHz) are obtained on channel **A** (Fig. 16(a)) and receive the information signal at the output channel **B** (Fig. 16(a)). From the graphs in Fig. 16(a), it can be seen that the signals coincide very well with each other. Fig. 16(b) shows the temporal diagrams of chaotic signals obtained by connecting the XSC1 oscilloscope to the chaos generators GS1 and GS2. Here, one can also see a good agreement between the graphs of chaotic oscillations. When connecting any channel of the XSC1 oscilloscope to a point in the diagram in Fig. 15, the temporal diagram of a mixed (or additive) chaotic signal transmitted to the receiver is observed (Fig. 16(c)). The phase portraits of the transmitted and received periodic signal are shown in Fig. 16(d), which indicates that the signal on the receiving side of the communication system is obtained without distortion.

4.2. The error dynamics in the parameters of certain circuit components

In this section, the question of whether or not the circuit can also keep synchronized by changing the parameters of a certain circuit component is investigated. A resistor, capacitor, and analog multiplier are chosen to carry out the error analysis for the proposed chaotic secure communication circuit.

(1) In these numerical experiments, the value of the resistor R_2, which corresponds to the change in the bifurcation parameter (Rayleigh number) in the system of Eq. (2), is changed. The R_2 value of the transmitting circuit and receiving circuit is R_2 = 1.724 kΩ. When the value of R_2 is chosen as R_2 = 1.69 kΩ (Rayleigh number R = 59) and R_2 = 1.43 kΩ (Rayleigh number R = 70) for the receiving part (GS2), the waveform and the phase diagram are shown in Fig. 17 and Fig. 18.

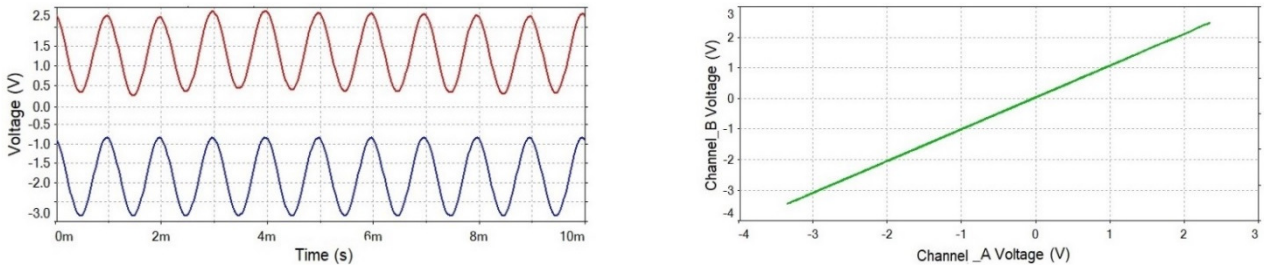

(a) The transmitting and receiving waveform (b) The synchronous phase diagram

Fig. 17 The resistor R_2 of the receiving circuit with an approximate 2% error

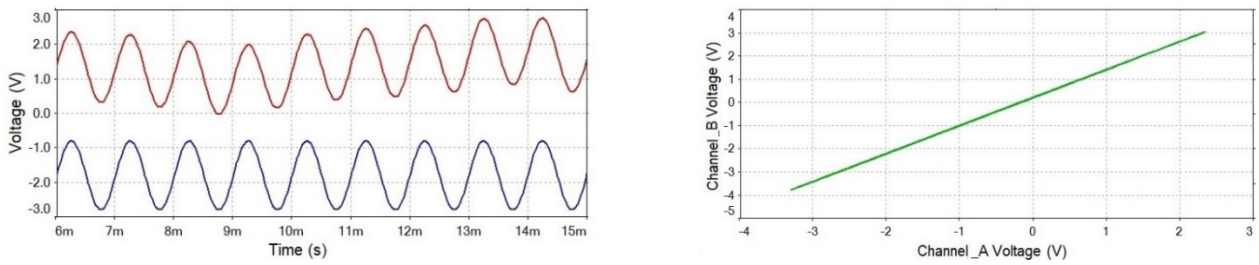

(a) The transmitting and receiving waveform (b) The synchronous phase diagram

Fig. 18 The resistor R_2 of the receiving circuit with an approximate 17% error

From the experimental results in Fig. 17 and Fig. 18, it can be seen that synchronization can be realized when the resistor R_2 of the receiving circuit has an error of 2% and above, and there is almost no noise. Therefore, the variation in the R_2 value of the receiving circuit has a negative impact on synchronization.

(2) The capacitor value C_1 of the transmitting circuit and receiving circuit is 100 nF. In these experiments, when the values of C_1 are chosen as 101 nF and 105 nF for the receiving part (GS2), the waveform and the phase diagram are shown in Fig. 19 and Fig. 20.

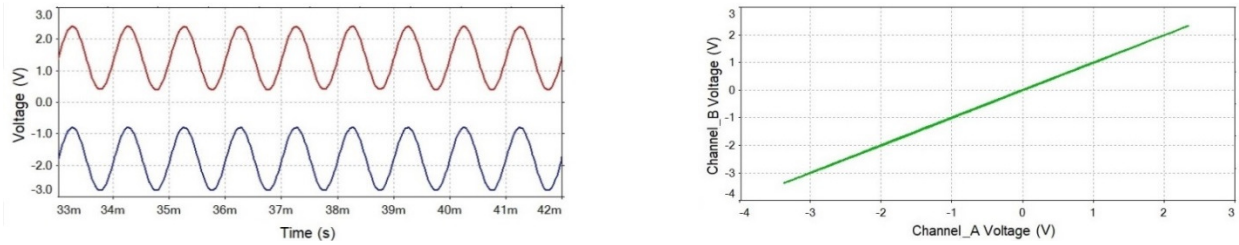

(a) The transmitting and receiving waveform (b) The synchronous phase diagram

Fig. 19 The capacitor C_1 of the receiving circuit with a 1% error

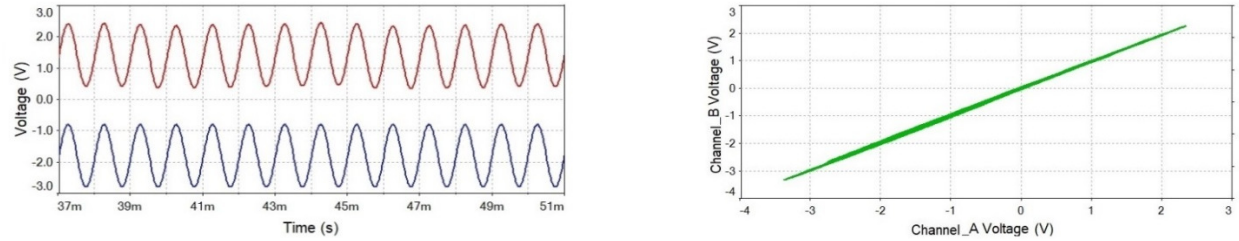

(a) The transmitting and receiving waveform (b) The synchronous phase diagram

Fig. 20 The capacitor C_1 of the receiving circuit with a 5% error

From the experimental results in Fig. 19 and Fig. 20, it can be seen that the synchronization can be implemented when a capacitor value of the receiving circuit has an error between 1% and 5%, but the noise is obvious. Therefore, the variation in the C_1 value of the receiving circuit has a positive impact on synchronization. The output gains of four analog multipliers for the transmitting and receiving parts are 0.1 V/V. In the experiments, when multipliers of the receiving circuit are chosen as 0.105 V/V and 0.11 V/V, the waveform and the phase diagram are shown in Fig. 21 and Fig. 22.

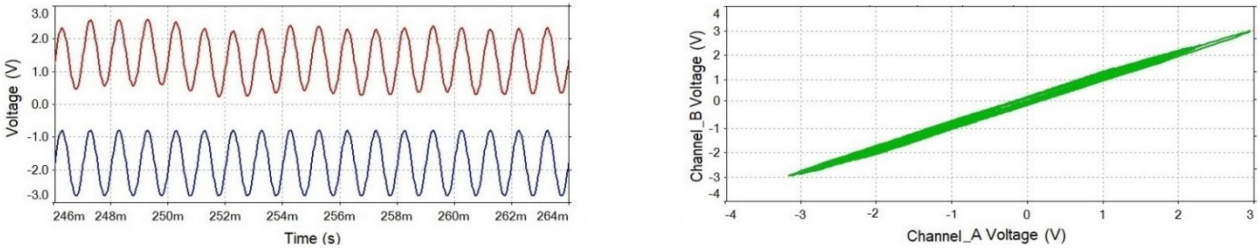

(a) The transmitting and receiving waveform (b) The synchronous phase diagram

Fig. 21 Analog multipliers of the receiving part with 0.5% error

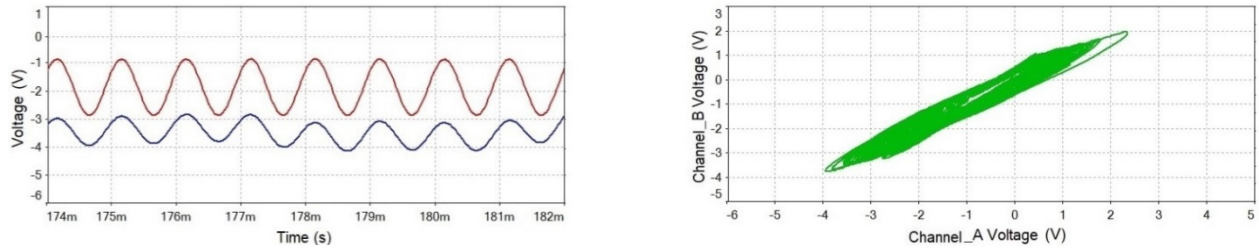

(a) The transmitting and receiving waveform (b) The synchronous phase diagram

Fig. 22 Analog multipliers of the receiving part with 1% error

It can be seen that the synchronization can be implemented when multipliers of the receiving part have a small error of 0.05%, but there is a small noise. When multipliers of the receiving part are chosen as 0.11 V/V, the waveform and the phase diagram are shown in Fig. 22. From the experimental results, it can be observed that the synchronization can be still realized when analog multipliers of the receiving part have an error of 1%, but the noise is obvious.

In addition, it is noted that for the new 6D generator, the choice of the analog multiplier is the most important. The sensitivity of the chaotic circuit to the initial value also requires selecting appropriate circuit components in the practical chaotic secure communication experiments. Thus, the simulation results confirm that the proposed electronic circuit of the new chaos generator can implement the effective transmission and reception of the signals.

5. Conclusions

In this work, the dynamic analysis of the new 6D chaotic system from the article [24] is extended. Hence, the following theoretical studies are conducted:

(1) The fundamental properties of the system such as Lyapunov exponents and Kaplan-Yorke dimension, as well as its phase portraits, are described in detail.

(2) An adaptive controller for stabilizing the proposed system with unknown parameters and the chaos synchronization of two identical chaotic systems is studied.

Then, using the theoretical outcomes mentioned above, the Matlab-Simulink and LabVIEW models are designed for the numerical simulation of nonlinear dynamics equations. The proposed dynamics equations describe the nonuniformly rotating convection of an electrically conductive fluid in a constant vertical magnetic field. Thus, an electronic circuit of a chaos generator is designed for a 6D chaotic system. The performance of this electronic circuit is tested in the MultiSim environment.

Considering the time diagrams and phase portraits obtained using the Matlab-Simulink and LabVIEW simulation, the following conclusions can be summarized:

(1) The oscillations arising in the chaotic system (Eq. (1)) have complex chaotic behavior.

(2) In the proposed 6D chaotic system, the Pecor-Carroll method is successfully applied for chaotic masking and signal decoding.

(3) The designed electronic circuit based on the proposed 6D chaotic system can be efficiently applied to chaotic secure communication since the transmitting signal is received without noise.

(4) The obtained electronic circuit of the chaos generator is efficient for chaotic secure communication because of its synchronization properties.

In the future, the proposed electronic circuit of a chaotic generator can be used as the main part of modern systems to receive and transmit information for masking and decrypting an information carrier. Experimental implementation of new chaos generators will be useful in designing multichannel devices for the secure transmission of information.

Acknowledgments

The authors are grateful to three anonymous reviewers for their valuable suggestions and comments.

Conflicts of Interest

The authors declare no conflicts of interest.

References

[1] F. Yu, et al., "Secure Communication Scheme Based on a New 5D Multistable Four-Wing Memristive Hyperchaotic System with Disturbance Inputs," Complexity, vol. 2020, pp. 1-16, January 2020.

[2] A. Ouannas, et al., "A Novel Secure Communications Scheme Based on Chaotic Modulation, Recursive Encryption and Chaotic Masking," Alexandria Engineering Journal, vol. 60, no. 1, pp. 1873-1884, December 2020.

[3] S. Wang, et al., "An Image Encryption Algorithm Based on a Hidden Attractor Chaos System and the Knuth-Durstenfeld Algorithm," Optics and Lasers in Engineering, vol. 128, Article no. 105995, May 2020.

[4] A. Sambas, et al., "A 3-D Multi-Stable System with a Peanut-Shaped Equilibrium Curve: Circuit Design, FPGA Realization, and an Application to Image Encryption," IEEE Access, vol. 8, pp. 137116-137132, July 2020.

[5] S. Vaidyanathan, et al., "A New Biological Snap Oscillator: Its Modelling, Analysis, Simulations and Circuit Design," International Journal of Simulation and Process Modelling, vol. 13, no. 5, pp. 419-432, January 2018.

[6] E. N. Lorenz, "Deterministic Non-Periodic Flow," Journal of the Atmospheric Sciences, vol. 20, pp. 130-142, March 1963.

[7] K. M. Cuomo, et al., "Circuit Implementation of Synchronized Chaos with Applications to Communications," Physical Review Letters, vol. 71, no. 1, pp. 65-68, August 1993.

[8] K. M. Ibrahim, et al., "Chaotic Behavior of the Rossler Model and Its Analysis by Using Bifurcations of Limit Cycles and Chaotic Attractors," Journal of Physics: Conference Series, vol. 1003, no. 1, Article no. 012099, May 2018.

[9] Y. Y. Hou, et al., "Rikitake Dynamo System, Its Circuit Simulation and Chaotic Synchronization via Quasi-Sliding Mode Control," TELKOMNIKA Telecommunication, Computing, Electronics, and Control, vol. 19, no. 4, pp. 1428-1438, August 2021.

[10] F. Hannachi, "Analysis, Dynamics and Adaptive Control Synchronization of a Novel Chaotic 3D System," SN Applied Sciences, vol. 1, no. 2, Article no. 158, February 2019.

[11] I. Pehlivan, et al., "A New Chaotic Attractor from General Lorenz System Family and Its Electronic Experimental Implementation," Turkish Journal of Electrical Engineering and Computer Sciences, vol. 18, no. 2, pp. 171-184, March 2010.

[12] Q. H. Alsafasfeh, et al., "A New Chaotic Behavior from Lorenz and Rossler Systems and Its Electronic Circuit Implementation," Circuits and Systems, vol. 2, no. 2, pp. 101-105, April 2011.

[13] S. Vaidyanathan, et al., "Analysis, Adaptive Control and Synchronization of a Seven-Term Novel 3D Chaotic System with Three Quadratic Nonlinearities and Its Digital Implementation in LabVIEW," Journal of Engineering Science and Technology Review, vol. 8, no. 2, pp. 130-141, April 2015.

[14] A. Sambas, et al., "Dynamics, Circuit Design and Fractional-Order Form of a Modified Rucklidge Chaotic System," Journal of Physics: Conference Series, vol. 1090, no. 1, Article no. 012038, September 2018.

[15] F. Q. Wang, et al., "Hyperchaos Evolved from the Liu Chaotic System," Chinese Physics B, vol. 15, no. 5, pp. 963-968, May 2006.

[16] M. W. Luo, et al., "Circuitry Implementation of a Novel Four-Dimensional Nonautonomous Hyperchaotic Liu System and Its Experimental Studies on Synchronization Control," Chinese Physics B, vol. 18, no. 6, pp. 2168-2175, June 2009.

[17] J. Lu, et al., "The Compound Structure of a New Chaotic Attractor," Chaos, Solitons, and Fractals, vol. 14, no. 5, pp. 669-672, September 2002.

[18] L. Xiong, et al., "Dynamical Analysis, Synchronization, Circuit Design, and Secure Communication of a Novel Hyperchaotic System," Complexity, vol. 2017, Article no. 4962739, 2017.

[19] L. Xiong, et al., "Circuit Implementation and Antisynchronization of an Improved Lorenz Chaotic System," Shock and Vibration, vol. 2016, Article no. 1617570, 2016.

[20] S. Vaidyanathan, et al., "Analysis, Control, Synchronization and SPICE Implementation of a Novel 4D Hyperchaotic Rikitake Dynamo System without Equilibrium," Journal of Engineering Science and Technology Review, vol. 8, no. 2, pp. 232-244, April 2015.

[21] S. Vaidyanathan, et al., "A 5D Hyperchaotic Rikitake Dynamo System with Hidden Attractors," The European Physical Journal Special Topics, vol. 224, pp. 1575-1592, July 2015.

[22] S. Vaidyanathan, et al., "A 5D Multi-Stable Hyperchaotic Two-Disk Dynamo System with no Equilibrium Point: Circuit Design, FPGA Realization and Applications to TRNGs and Image Encryption," IEEE Access, vol. 9, pp. 81352-81369, June 2021.

[23] E. Tlelo-Cuautle, et al., Optimization of Integer/Fractional Order Chaotic Systems by Metaheuristics and Their Electronic Realization, Boca Raton: CRC Press, 2021.

[24] M. I. Kopp, et al., "Magnetic Convection in a Nonuniformly Rotating Electroconducting Medium," Journal of Experimental and Theoretical Physics, vol. 127, no. 6, pp. 1173-1196, July 2018.
[25] G. Benettin, et al., "Lyapunov Characteristic Exponents for Smooth Dynamical Systems and for Hamiltonian Systems: A Method for Computing All of Them," Meccanica, vol. 15, no. 1, pp. 9-20, March 1980.
[26] A. Wolf, et al., "Determining Lyapunov Exponents from a Time Series," Physica D: Nonlinear Phenomena, vol. 16, no. 3, pp. 285-317, July 1985.
[27] M. Sandri, "Numerical Calculation of Lyapunov Exponents," The Mathematica Journal, vol. 6, pp. 78-84, January 1996.
[28] H. Binous, et al., "An Improved Method for Lyapunov Exponents Computation," https://library.wolfram.com/infocenter/MathSource/7109/, March 09, 2008.
[29] L. M. Pecora, et al., "Synchronization in Chaotic Systems," Physical Review Letters, vol. 64, no. 8, pp, 821-824, March 1990.
[30] R. W. Larsen, LabVIEW for Engineers, Upper Saddle River: Prentice Hall, 2011.